PAPER

Check for updates

Poly(vinyl chloride) microplastics induce structural and functional alterations in myoglobin

Souvik Ghosal, [a] Sagar Bag [b] and Sudipta Bhowmik *[ab]

Microplastics (MPs) pollution represents a global concern for biodiversity conservation, ecosystem and public health. The poly(vinyl chloride) Microplastics (PVC-MPs) are one of the dominant pollutants in both terrestrial and aquatic ecosystem. Myoglobin (Mb) is an important intracellular oxygen-binding protein found in mammals' hearts and skeletal muscles. Mb act as an oxygen transporter and storage material in muscle cells. Due to molecular inertness and excellent accessibility to organisms, PVC-MPs are degraded slowly in the atmosphere and can accumulate in the mammalian bloodstream, posing major health risks. In this study, under simulated physiological conditions, the interaction between the emerging pollutant PVC-MPs and Mb was analysed using multispectroscopic studies. From these studies, it has been found that PVC-MPs may bind to Mb during transportation and metabolic activities. Because of their tiny size, PVC-MPs may bind with Mb once they enter the bloodstream, altering the structure and physiological function of Mb. These results also suggest that electrostatic forces were the primary factor behind the interaction between PVC-MPs and Mb. Additionally, the results further showed that PVC-MPs significantly altered the microenvironment and secondary structure of Mb, which decreased the α-helix. This study clarifies the possible molecular toxicity of PVC-MPs in addition to provide crucial insight into the intermolecular interaction between PVC-MPs and Mb.

1. Introduction

Pollution is the result of unfavourable changes in our environment that negatively impact humans, animals, and plants. The degree of harmful impact on human health is determined by the kind and concentration of a pollutant. Microplastic pollution is one of the greatest threats to the global population today.[1,2] Microplastics (MPs) are defined as a heterogeneous mixture of differently shaped materials referred to as fragments, fibres, spheroids, granules, pellets, flakes or beads, in the range of 0.1–5000 μm and nano plastics from approximately 1 to 100 nm (0.001–0.1 μm).[3] MPs contamination has grown in importance as a study topic in ecology and environmental science.[4,5] MPs smaller than 150 μm have the ability to move to the blood and lymphatic systems, resulting in systemic exposure. However, it is predicted that less than 0.3% of these MPs will be absorbed. Only MPs smaller than 20 μm may be able to enter some organs, whereas MPs smaller than 1 μm may be able to enter all organs and cellular membranes before dispersing throughout the body.[6,7] In human, 7.91–9.45 MPs per g (43.52–60.11 μm) found in intestine which comprised of mostly PVC.

2.7–18 MPs per g (5–307.2 μm) found in placenta which comprised of mostly PVC, PE, PS, PET, PBS. 0.23 MPs per ml (96.19 μm) found in semen which comprised of mostly PVC, PE, PA, PS. 1.6 μg ml^{-1} (≥700 nm) found in blood which comprised of mostly PET, PE, PS.[8] Therefore, it is crucial to continue researching the potential toxicological effects of MPs on biomacromolecules with crucial physiological roles, as swallowed MPs have the potential to reach the organs and blood circulation system.

According to a study, poly(vinyl chloride) microplastics interacted with human serum albumin and altered its secondary structure.[9,10] A different study proves that polystyrene nano plastics interacted with diastase α-amylase and induce a conformational structural change, also altered its enzymatic activity.[11] Another study done by Ghosal *et al.* 2024 proves that microplastics interacted with human alpha synuclein protein, altered protein's structure and promote amyloidogenic oligomer.[12] Recently a study done by Yang *et al.* 2023 shows that microplastics can be found in human cardiac muscle and that increases the risk of cardiac diseases.[13,14] An essential intracellular O$_2$-binding protein present in the heart and skeletal muscle of mammals is called Myoglobin (Mb). Mb is a globular protein that dissolves in water and has 153 amino acids. Its centre is hydrophobic, and it has eight alpha helices. One prosthetic group is present in each Mb molecule, and it is put into a protein's hydrophobic cleft. One centrally coordinated iron atom, typically in the (2$^+$) oxidation state, is present in each

a Mahatma Gandhi Medical Advanced Research Institute (MGMARI), Sri Balaji Vidyapeeth (Deemed to be University), Pondy–Cuddalore Main Road, Pillaiyarkuppam, Pondicherry 607402, India

b Department of Biophysics, Molecular Biology and Bioinformatics, University of Calcutta, 92, A.P.C. Road, Kolkata 700009, India. E-mail: su_sudipta@yahoo.co.in; sbbmbg@caluniv.ac.in

heme residue. Mb serves as a transporter and a store of oxygen in muscle cells.[15,16] Therefore, Mb serves as a crucial link between the capillary supply of O_2 provided by circulating haemoglobin and the O_2-consuming cytochromes for oxidative phosphorylation in the mitochondrial membrane.[17] If the Mb from cardiac muscle interacted with microplastics, there must be some impact on the structure of Mb induced by microplastics. So, in this study we want to investigate the interaction between microplastics [PVC, PE, and PS-MPs] and Mb.

In this study, we hypothesized that MPs are binding to Mb and causes the structural alterations of Mb. To investigate this hypothesis, a combination of spectroscopic techniques was used to estimate the binding behaviour of 3 different microplastics (PE, PVC and PS-MPs) with Mb under simulated physiological conditions (pH = 7.4, temperature = 37 °C). The most commonly used and produced plastics are PE, PVC, PS. In aquatic environment they are present in highest number and this three microplastics presence has been reported in almost all body parts of human being.[18] Because of this, we have selected the indicated microplastics. Here, fluorescence spectral data were mathematically analysed to determine the binding constants of Mb with PVC-MPs at various temperatures. Thermodynamics was analysed to determine the major binding forces involved in molecular interactions between Mb and PVC-MPs. In addition, Circular Dichroism (CD), Ultra Violet-visible Absorption Spectroscopy, thermal melting and Fourier Transform Infrared Spectroscopy (FT-IR) were employed to investigate the effects of PVC-MPs on the structural properties of Mb.

2. Materials and methods

2.1. Materials

Both Mb lyophilized powder and poly(vinyl chloride) microplastics, polyethylene microplastics and polystyrene microplastics were purchased from Sigma Aldrich in the United States. Phosphate Buffer Saline (PBS) (50 mM KCL, 10 mM KH_2PO_4, and 1 mM K_2EDTA) was used to dissolve Mb. By using spectrophotometric absorbance and taking into account the ε of Mb at 280 nm (13 980 M^{-1} cm^{-1}), Mb concentration was determined.[19,20] Mb is present in experimental stock concentrations of 100 μM. Three microplastics quality is standard controlled (MQ100). The form of PVC-MPs is powder, density is 1.4 g ml^{-1}. The form of PE-MPs is powder, density is 0.94 g ml^{-1}. The form of PS-MPs is aqueous suspension particles; density is 1.05 g cm^{-3}. The PVC-MPs, PE-MPs and PS-MPs stock solution was prepared as per our previous work (Fig. S11).[12]

2.2. Microplastics characterization

Physical properties like shape, size, morphology of 3 microplastics were examined under FE-SEM (JEOL MAKE, Model: JSM-7500F) by fixing a thin film of MPs on copper grid. Prior to SEM analysis, the sample was coated with gold using sputter coater.[21]

The hydrodynamic diameter, and polydispersity index (PDI) of the MPs in aqueous suspension were estimated using dynamic light scattering (DLS) and ζ-potential measurements.

For analysis MPs were suspended in deionized (DI) water at 25 °C in a Malvern Zetasizer Nano ZSP series. Each sample was measured in disposable folded capillary micro-cuvettes three consecutive times with a 2 s delay between measurements. The duration of the measurements varied from 50 to 100 s depending on the dispersity of the sample. The identity of the MPs was confirmed using FT-IR spectroscopy.[22]

For ^{1}H-NMR analysis, MP particles have to be dissolved in a suitable deuterated solvent. Deuterated dimethyl sulfoxide (DMSO-d6) (99.8 at% D) from Deutero, Germany, was used. Starting from a stock solution, five different concentrations of MP particles were prepared for calibration. In order to prepare the model samples, a defined amount of PE, PVC and PS particles was transferred to a glass vessel and dissolved in the solvent. After dissolving, the sample solutions or calibration solutions were transferred to 5 mm NMR tubes for ^{1}H-NMR measurements. To avoid contamination of the samples, all glassware was washed with water, acetone and distilled water and was dried at 60 °C for at least 24 h. During sample preparation samples were covered whenever possible. In addition, care was taken to close the lab coat (100% cotton) when working with the samples in order to avoid contamination with polymer fibres from clothes. ^{1}H-NMR experiments were performed on a JEOL ® 500 spectrometer with a 500 MHz 5- mm TH ATM probe head and a pulse of 90° was used. All measurements were conducted at room temperature.[23]

2.3. Steady-state spectrofluorometric studies

The fluorescence emission spectra of Mb were measured on a Horiba scientific fluorescence spectrometer and one-centimetre quartz cuvette. Investigations were carried out by holding Mb concentration constant at 15 μM (Ex.: 280 nm; Em.: 340 nm) and then titrating with escalating concentrations (0–100 μg ml^{-1}) of PVC-MPs, PE-MPs, and PS-MPs.[24,25]

2.3.1. UV-vis absorption spectroscopy.
Hitachi UH5300 was used to measure the UV-vis absorption spectra of Mb (3 μM) in the absence and presence of PVC-MPs, PE-MPs, and PS-MPs (0–100 μg ml^{-1}).[24,26]

2.3.2. Thermal melting.
Thermal denaturation experiments were performed using 15 μM Mb in the absence and presence of 50 μg ml^{-1} PVC-MPs, according to our previous work.[24] For UV melting we have used double distilled water (pH 7.4) as media.

2.4. Circular Dichroism spectroscopy

The Jasco J-1500 CD Spectrometer was used to do the CD measurements of Mb (3 μM) in the absence or presence of PVC-MPs (20–100 μg ml^{-1}) according to our previous work.[12]

2.5. Fourier transform infrared spectroscopy (FT-IR)

The FT-IR spectra of Mb (3 μM) in the absence and presence of PVC-MPs (100 μg ml^{-1}) were assessed using a Spotlight 400 FT-IR spectrometer (PerkinElmer, UK) at room temperature (298 K).[12]

2.6. Statistical investigation

All the experiments in this present investigation were performed in triplicate. All the experimental outcomes were evaluated at a significance level of $p < 0.05$. The OriginPro application in Origin-2019b software was utilized to analyse and export the graphs/curves.

3. Results and discussion

3.1. Microplastics characterization

FE-SEM, which analyses the micro/nanostructure of particles using an electron beam, can be used to determine the surface morphology of PE-MPs (a), PVC-MPs (b), and PS-MPs (c) at scale bar 500 μm, 100 μm, and 5 μm respectively. The average size of plain PE-MPs (a), PVC-MPs (b), and PS-MPs (c) was observed to be ~19.2 μm, ~10.7 μm, and ~953 nm respectively (Fig. S3–S5).[21]

In this study, we characterized the number (percent) *versus* size peaks from DLS measurements (Fig. S6) shows hydrodynamic size range of the respective MPs (PE ~10 μm ± 19.55, PVC ~8 μm ± 15.03, and PS ~900 nm ± 29.25) suspended in DI water at 25 °C. The particle size determined by DLS measurement showed size variation from SEM images, as DLS indicates hydrodynamic diameter of dispersed MPs in suspensions, which depend on the thickness of the hydration/solvation layer, thus varying from the core particle size. Polydispersity index (PDI)-1, shows heterogeneity of particle sizes in all three MP samples.[22]

The FTIR spectrum of PE-MPs exhibits characteristic absorption bands that can be used for identification and analysis. 2913 cm^{-1}: this peak corresponds to the asymmetric stretching vibration of the CH$_2$ (methylene) groups. 2845 cm^{-1}: this peak is attributed to the symmetric stretching vibration of the CH$_2$ groups. 1465 cm^{-1}: this peak is associated with the bending vibrations of the CH$_2$ groups. 718 cm^{-1}: this peak is related to the rocking vibration of the CH$_2$ groups (Fig. S7a).[27] For PVC-MPs, Bands around 2911 cm^{-1} and 2836 cm^{-1} are attributed to CH$_2$ asymmetric stretching. Bands around 1430 cm^{-1} and 1332 cm^{-1} are associated with CH bending and deformation modes. A band around 614 cm^{-1} or 834 cm^{-1} is indicative of the C–Cl bond in PVC. A band around 1096 cm^{-1} is assigned to the C–C bond in the PVC backbone. A band around 1254 cm^{-1} can be attributed to CH rocking vibrations. A band around 959 cm^{-1} is related to *trans* C–H wagging (Fig. S7b).[28] The major characteristic peaks at 3026, 2920, 2850, 1598, 1492, and 752 wavenumbers are seen in the pure PS-MPs samples (Fig. S7c). The peaks at 3026 and 1598 cm^{-1} represent aromatic C–H stretching and C=C vinyl group, respectively. Characteristics peaks at 2920 and 2850 cm^{-1} are related to CH$_2$ asymmetric stretching and CH$_2$ symmetric stretching respectively. The peak at 1492 cm^{-1} is due to deformational vibrations of benzene ring whereas the peak at 752 cm^{-1} suggests deformational vibrations of substituted benzene derivative.[29]

NMR spectroscopy is a powerful tool for the structural analysis of organic and polymeric compounds. ^{1}H NMR spectra of PE typically show characteristic signals around 1.12 and 0.74–0.70 ppm, corresponding to the methylene and methyl groups, respectively, in the polymer chain (Fig. S8). Fig. S9 shows a ^{1}H-NMR spectrum of PVC powder. The signal of 4.6–4.2 ppm (H1) corresponds to the α-Cl H atoms and the signal in the range of 2.5–2.1 ppm (H2) to the β-Cl H atoms. Fig. S10 PS exhibited proton signals in the range of 7.20 to 6.20 ppm (PS-Ha, Hb). Usually, these signals are assigned to PE, PVC, and PS in literature.[23,30,31]

3.2. Fluorescence quenching study

One effective method for examining the dynamic alterations and molecular interactions of proteins is fluorescence spectroscopy, which can yield important details about the binding process.[32] It is known that Mb contains three fluorophores with significant intrinsic fluorescence: Trp (Tryptophan), Tyr (Tyrosine), and Phe (Phenylalanine) residues. The presence of two Trp residues, however, is primarily responsible for the intrinsic fluorescence of Mb excited at 280 nm. The poor quantum yield of Phe residues and the nearly complete quenching of Tyr residues' fluorescence significantly reduced their contribution to Mb's fluorescence.[33] Therefore, the binding interaction of PVC-MPs with Mb was investigated using fluorescence emission spectra. The fluorescence emission spectra of Mb at 298 K with various MPs present are displayed in Fig. 1 and S1. After being excited with 280 nm, Mb exhibits a significant fluorescence emission peak at 328 nm, as can be seen. In contrast, PVC-MPs have been reported to disclose no emission, suggesting that PVC-MPs had no effect in exciting Mb.[34] Furthermore, the addition of PVC-MPs clearly quenched the fluorescence intensity of Mb, although the introduction of PE-MPs and PS-MPs barely affected the peak's position or intensity. Due to PVC-MPs suitable dispersibility in water, this finding suggested that PVC-MPs might affect the microenvironment and cause the fluorescence quenching of Mb. Thus, it is investigated how PVC-MPs affect the fluorescence intensity of Mb, as seen in Fig. 1. The reduction in intensity of fluorescence demonstrated that the binding relationship between PVC-MPs and Mb may efficiently stifle Mb's intrinsic fluorescence and further modify the microenvironment around Mb. Lesser change seen in fluorescence intensity when PE-MPs and PS-MPs added into Mb (Fig. S1).

3.3. Fluorescence quenching mechanism

It's well known that fluorescence quenching, which may be brought about by an array of chemical reactions including energy transfer, ground-state complex formation, excited-state processes, and collisional quenching, represents the reduce in the fluorescence quantum yield of a fluorophore. Dynamic and static quenching, which are brought about by collisions and the creation of ground-state complexes, respectively, are two types of quenching that occur in fluorescence. Furthermore, the primary distinction between static and dynamic quenching is their reliance on temperature. Raising the temperature during static quenching will lessen complicated stability and further lower static quenching constants. In contrast, in the dynamic quenching process, it is expected that the dynamic quenching
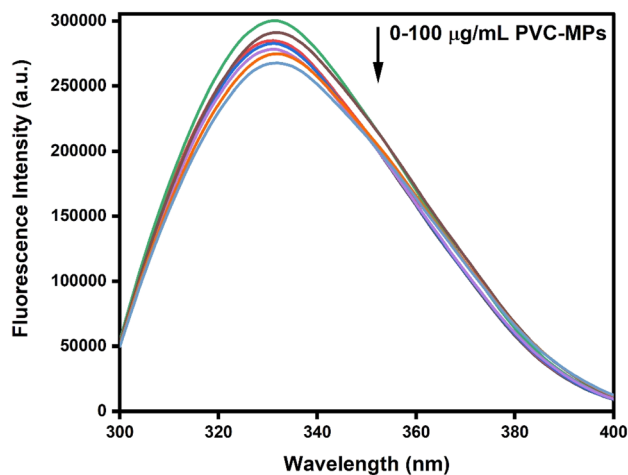
Fig. 1 Steady-state fluorescence of Mb in absence and presence of PVC-MPs in different concentration. [Mb] = 15 μM. [PVC-MPs] = 0–100 μg ml^{-1}, pH = 7.4, T = 298 K.

constants would rise as the temperature rises due to quicker diffusion and greater collisions. Therefore, using the Stern–Volmer equation, the fluorescence emission spectra at 298 K, 304 K, and 310 K may be used to analyse the fluorescence quenching mechanism of Mb caused by PVC-MPs:[35–37]

$$\frac{F_0}{F} = 1 + K_q \tau_0 c_q = 1 + K_{SV} c_q \qquad (1)$$

where c_q is the quencher concentration, τ_0 is the mean lifetime of a molecule without a quencher (10^{-8} s), K_{SV} stands for the constant of Stern–Volmer, K_q is the constant of quenching rate of a biomolecule, and F_0 and F stands for the steady-state fluorescence intensities of Mb in the absence and presence of poly(vinyl chloride) microplastics, respectively.[35,36] The Stern–Volmer plots at 298 K, 304 K, and 310 K are displayed in Fig. 2a. The associated values of K_{SV} and K_q are thus deduced and are presented in Table 1. These results showed that, as opposed to dynamic collision, which mostly followed a static quenching process, the fluorescence quenching of Mb produced by PVC-MPs was derived from the creation of ground state complex (Mb-PVC-MPs). The primary cause of the drop in fluorescence intensity during static quenching is thought to be the quencher's interaction with the fluorophore, which results in the development of a ground-state complex that is non-fluorescing. This may be further explained using the Lineweaver–Burk equation.[38]

$$(F_0 - F)^{-1} = F_0^{-1} + K_a^{-1} F_0^{-1} C_q^{-1} \qquad (2)$$

Here, K_a is the static quenching binding constant, F_0, F, and C_q stand for the same meanings as in eqn (1), and thus illustrates the dose-effect connection in the binding response at equilibrium state. The binding constants K_a was therefore determined at various temperatures by analysing the graphs of F_0/F against C_q (Fig. 2b), which are shown in Table 1. There was a clear trend for K_a to drop as temperature increased, suggesting that an unstable complex between Mb and PVC-MPs developed that was

inversely linked to temperature increases. This combination gave rise to Mb's fluorescence quenching.[39,40]

3.4. Study of apparent binding constant and number of binding sites

The following equation can be used to deduce K_A (apparent binding constant) and n (number of binding sites) in static quenching:

$$\log\left[\frac{F_0 - F}{F}\right] = \log K_A + n\log C_q \qquad (3)$$

where n is the number of binding sites on each Mb molecule, K_A is the apparent binding constant of the interaction between PVC-MPs and Mb, and C_q, F_0, and F are the same as in eqn (1).[41,42] Thus, as shown in Fig. 2c and Table 1. K_A and n may be found from the intercept and slope, respectively, in the plots of $\log[(F_0 - F)/F]$ against $\log C_q$. The data indicates that there were several binding sites in Mb with a high affinity for binding with PVC-MPs, as evidenced by the binding number of PVC-MPs with Mb of 1.30 at 298 K and K_A of 9.85×10^4 M^{-1}. PVC-MPs demonstrated a higher affinity for binding Mb, which might cause serious harm to Mb. Therefore, these findings further supported the strong binding association between PVC-MPs and Mb, as did the fluorescence quenching data. PVC-MPs have the ability to cause more severe harm *in vivo* once they reach the bloodstream and bind with Mb. Protein structure and physiological function will be disrupted, and the blood will spread to all organs.

3.5. Thermodynamics and binding forces analysis

The binding interactions of small molecules with macromolecules are mostly dominated by 4 types of noncovalent interactions: hydrophobic interaction forces, van der Waals forces, electrostatic interaction, and numerous hydrogen bonds. The major contact forces involved in the binding reaction may be explained by the signs and magnitudes of thermodynamic parameters like H (enthalpy) and S (entropy), according to Ross' study. From a thermodynamics perspective, $\Delta H > 0$ & $\Delta S > 0$ indicates that the hydrophobic interaction is the main drive; $\Delta H < 0$ & $\Delta S > 0$ indicates that the electrostatic force is important; $\Delta H < 0$ & $\Delta S < 0$ indicates that the van der Waals force, or hydrogen bond, is the dominant force. Therefore, the temperature dependent thermodynamic parameters were determined at 298 K, 304 K, and 310 K to show the binding forces of PVC-MPs with Mb. Furthermore, during these temperatures, there won't be any noticeable variations in the enthalpy change (ΔH) or structural changes in Mb. As a result, the binding reaction's enthalpy (H) may be thought of as a constant. The Van't Hoff equation may then be used to derive the ΔH (enthalpy change) as well as the ΔS (entropy change):[24,43–45]

$$\ln K_A = -\frac{\Delta H^\circ}{RT} + \frac{\Delta S^\circ}{R} \qquad (4)$$

where temperature is the T (298 K, 304 K, & 310 K), R is gas constant (8.314 J mol^{-1} K^{-1}), and K_A is apparent binding constant at the pertinent temperature. Thus, the slope and
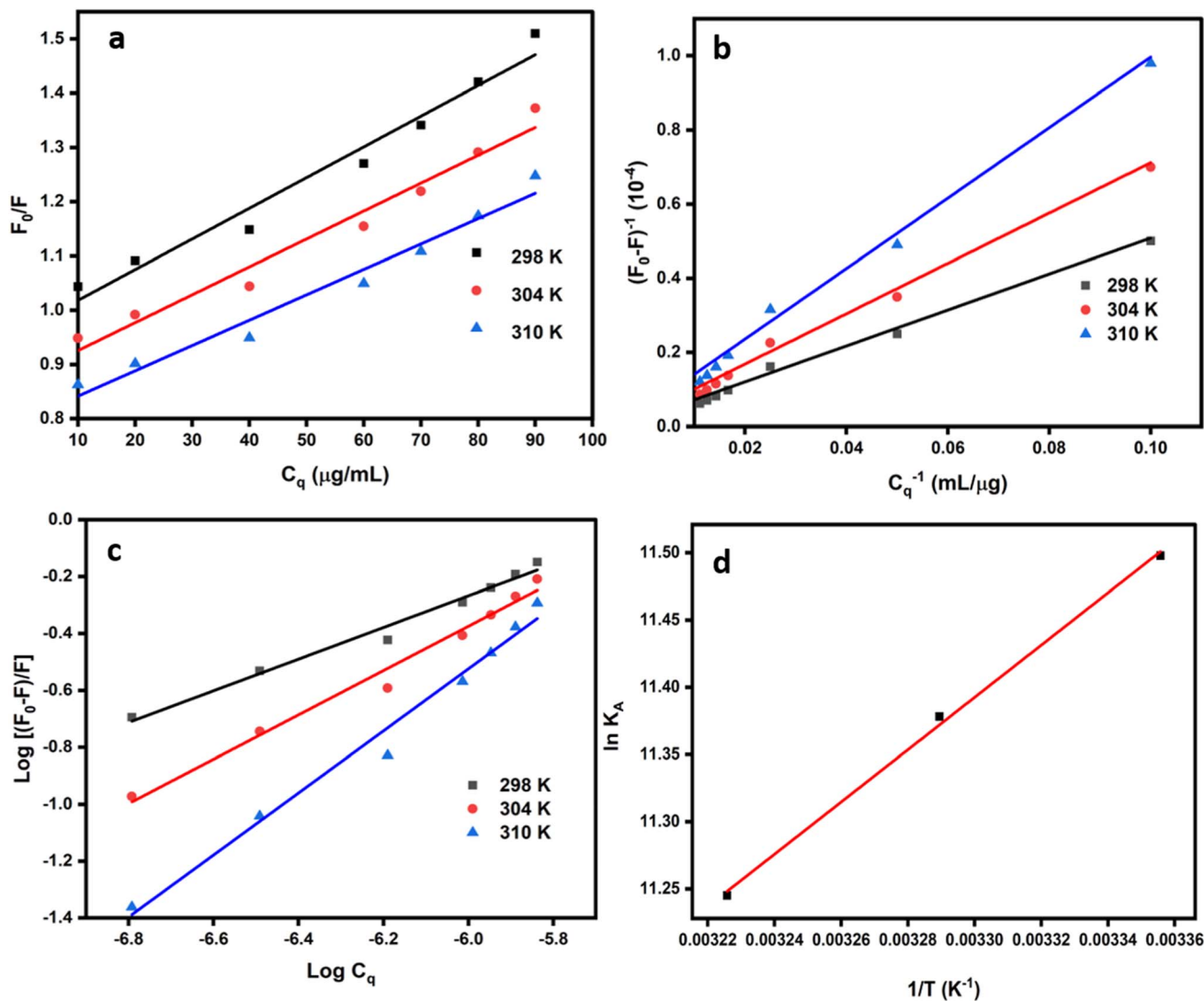
Fig. 2 (a) Stern–Volmer plots for the fluorescence quenching of Mb by PVC-MPs; (b) Lineweaver–Burk plots for the fluorescence quenching of Mb by PVC-MPs; (c) double logarithm plots for the fluorescence quenching of Mb by PVC-MPs; (d) Van't Hoff plot for the fluorescence quenching of Mb by PVC-MPs. [Mb] = 15 μM. [PVC-MPs] = 0–100 μg ml^{-1}, pH = 7.4, T = 298 K.

intercept in the Van't Hoff plot of ln K_A vs. $1/T$, respectively, yield ΔH and ΔS. There was a strong linear correlation between ln K_A & $1/T$, as seen in Fig. 2d. After that, the ΔG (free energy change) may be calculated using the relationship that follows:

$$\Delta G° = \Delta H° - T\Delta S° = -RT\ln K_A \qquad (5)$$

Hence, the thermodynamic data were computed and shown in Table 1 using the apparent binding constants K_A that were found using eqn (3). As can be observed, the negative sign of the

ΔG values suggests that PVC-MPs and Mb interacted spontaneously during binding. Furthermore, the exothermic reaction was followed by the binding contact between PVC-MPs and Mb, as shown by the positive sign of ΔS and negative value of ΔH. In the meanwhile, it was shown that electrostatic forces dominated the formation of the PVC-Mb complex and that entropy mostly drove the binding interaction. Consequently, our findings supported the idea that electrostatic forces had a significant role in the formation of a stable PVC-Mb complex.

Table 1 Binding parameters and thermodynamic parameters of PVC-Mb at different temperatures

T (K)	K_q (10^{11} M^{-1} S^{-1})	K_a (10^4 M^{-1})	K_A (10^4 M^{-1})	n	$\Delta G°$ (KJ mol^{-1})	$\Delta H°$ (KJ mol^{-1})	$\Delta S°$ (J mol^{-1} K^{-1})
298	3.0 ± 0.18	10.0 ± 1.22	9.85 ± 0.61	1.30 ± 0.1	−28.49 ± 0.21	−16.17 ± 0.15	41.35 ± 1.02
304	1.9 ± 0.13	5.8 ± 0.37	8.74 ± 0.65	1.11 ± 0.08	−28.74 ± 0.36		
310	0.6 ± 0.2	3.9 ± 0.75	7.65 ± 0.60	1.04 ± 0.05	−28.98 ± 0.16		

3.6. Conformational change of Mb induced by poly(vinyl chloride) microplastics

As previously established, while PVC-MPs binding to Mb can cause the protein to undergo fluorescence quenching through the formation of a complex, the impact of the binding interaction on Mb's secondary structure and/or microenvironment remained a mystery. Thus, to learn more about the variations in secondary structure and microenvironment in Mb, multi spectroscopic methods were used.

3.7. Ultra violet-visible absorption spectroscopy

The UV-vis absorption technique is a well-known and efficient method for looking for structural alterations in molecules. The UV-vis absorption spectra of Mb at various PVC–MPs concentrations are displayed in Fig. 3. In the blue wavelength region of the visible spectrum, the Soret band has a prominent peak. The Soret band forms as a result of an electron dipole shifting that permits π–π^* transitions, which are particularly prevalent in porphyrin compounds.[46–48] With UV-vis spectroscopy, a number of studies involving porphyrin-containing moiety may be carried out at the matching Soret band wavelength (409 nm). The absorption spectra of Mb (3 μM) show two peaks: the phenyl group of the Tyr and Trp residues causes one peak at 280 nm, and the porphyrin-Soret band (π–π^* transition) at 409 nm is created by the heme moiety inserted in the hydrophobic cavity of the protein. The modest absorption signal at around 280 nm may be used to identify three aromatic amino acids that are hidden inside the molecular structure: Trp, Tyr, and Phe.[24] Both the 409 and 280 nm band of Mb (3 μM) showed a decrease in intensity as the quantity of PVC-MPs (0–100 μg ml^{-1}) increased (Fig. 3). This result suggests that there is a complex formation between PVC-MPs and Mb. As a consequence, Mb's absorbance was reduced because a ground-state PVC-Mb complex with the same absorption peaks as Mb was formed. The interaction of PVC-MPs molecules may have exposed the

Mb's heme group, causing a change in its microenvironment and the entry of aqueous medium, as indicated by the reduction in 409 nm absorbance intensity. The Mb protein may undergo further folding modifications as a result of aromatic acid exposure to an aqueous environment, peptide strand extension, and disruption of the microenvironment and conformation of the residues at 280 nm by PVC-MPs, as shown by the reduction in 280 nm absorbance intensity. The UV-vis absorption spectra of Mb at various PE-MPs and PS-MPs concentrations are displayed in Fig. S2. In the presence of increasing concentration of the PE-MPs and PS-MPs (0–100 μg ml^{-1}), lesser change seen in both of the intensity of 409 and 280 nm band of Mb (3 μM) was observed.

3.8. Thermal melting analysis

Thermal denaturation tests (UV melting) were a dependable technique for examining the binding of PVC-MPs to Mb proteins. We also investigated the effect of PVC-MPs on Mb stability by thermal melting. Every visible transition was examined at the halfway point of the melting curve using T_m analysis. Utilising Mb protein absorbance at 280 nm, T_m values were determined.[49]

In this experiment, Mb (15 μM) exhibits T_m (melting temperature) at around 88.13 ($\pm$1.54)° Centigrade. In the presence of PVC-MPs, T_m value of Mb was increased to 91.68 ($\pm$1.98)° Centigrade at the concentration of 50 μg ml^{-1} of PVC-MPs. So, there is some gradual enhancement of T_m value of Mb (~3.55° Centigrade) with rising concentration of PVC-MPs. Therefore, it can be stated that PVC-MPs has stabilization effect on Mb (Fig. 4).

3.9. Circular dichroism (CD) spectroscopy

Using CD, the secondary structures of proteins as well as their conformational changes in diverse contexts and protein-ligand complexes have been investigated. In the far UV region (250 to
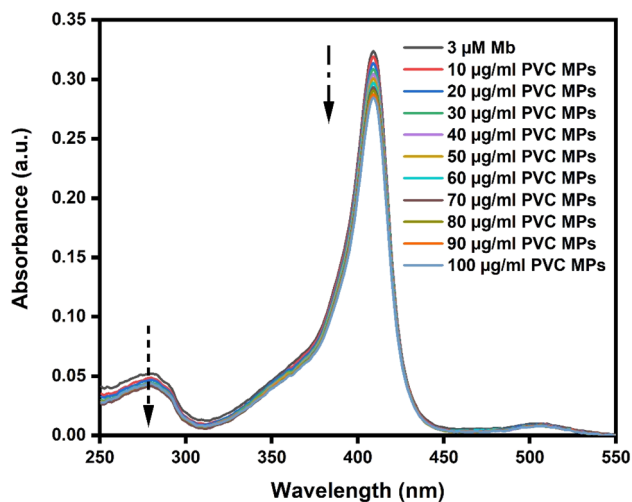

Fig. 3 UV-vis of Mb in absence and presence of PVC-MPs in different concentration. [Mb] = 3 μM. [PVC-MPs] = 0–100 μg ml^{-1}, pH = 7.4, T = 298 K.
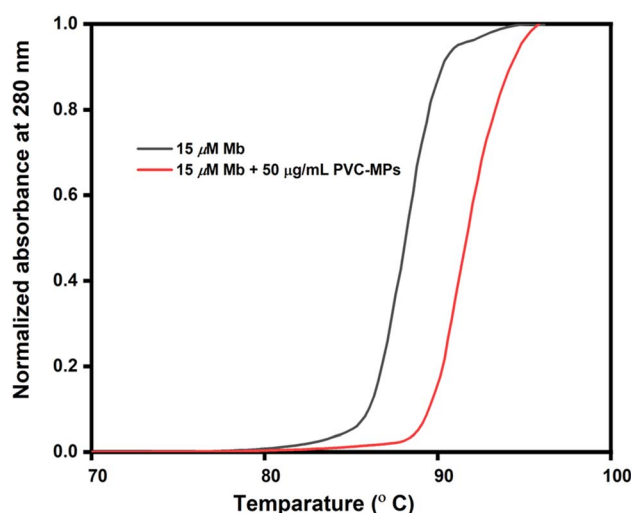

Fig. 4 Melting graph of Mb in the absence and presence of PVC-MPs. [Mb] = 15 μM. [PVC-MPs] = 50 μg mL^{-1} pH^{-1} = 7.4.
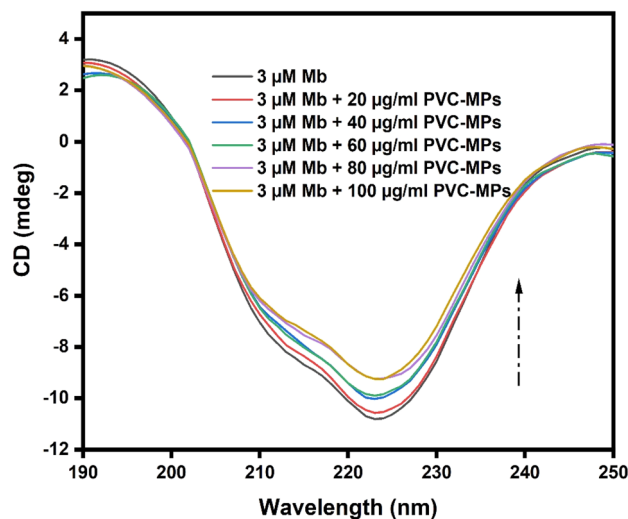
Fig. 5 CD spectra of Mb in the absence and presence of PVC-MPs in different concentration. [Mb] = 3 μM. [PVC-MPs] = 0–100 μg ml^{-1}, pH = 7.4, T = 298 K.
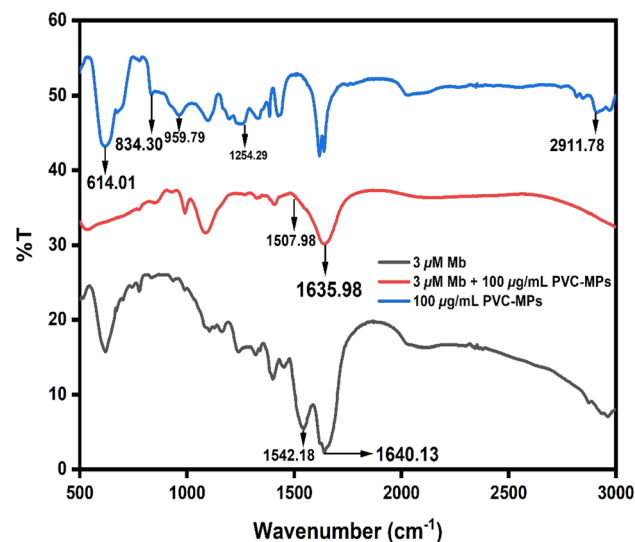

Fig. 6 FT-IR spectra of Mb in the absence and presence of PVC-MPs. pH = 7.4, T = 298 K.

190 nm), the Mb exhibits two negative peaks at around 208 and 222 nm, which are mostly due to the secondary structure of proteins. They are primarily mostly α-helices. The 208 nm band corresponds to the π–π* transition of the α-helix due to the transition of the peptide bond, whereas the 222 nm band is generated by the $n \rightarrow \pi$ * transition for both the helix and random coil complexes.[50–52] The α-helixes will change in accordance with any changes to the negative peaks. Upon successive addition of PVC-MPs (20–100 μg ml^{-1}) to a fixed concentration of Mb (3 μM), we found significant decrease in Mb's band intensity without a discernible wavelength shift, indicating that PVC MPs altered Mb's secondary structure by reducing the α-helix's extent (Fig. 5). Furthermore, Mb's helicity reduced as the concentration of PVC-MPs increased, suggesting that greater concentrations of PVC-MPs can more severely degrade Mb's secondary structure.

This outcome is consistent with the other spectroscopic findings that were previously mentioned. Furthermore, Mb's CD spectra with and without PVC-MPs had similar shapes, indicating that Mb's structure after binding with PVC-MPs was primarily α-helix.

The percentages of secondary structures in Mb with and without PVC-MPs are displayed in Table 2. It is evident that Mb's α-helix, anti-parallel β sheet, parallel β sheet, turn, and

random coil all changed considerably from native Mb to Mb in contact with PVC-MPs. Furthermore, it was observed that as the concentration of PVC-MPs increased, the contents of random coil increased, β-turn contents increased, and the contents of α-helices decreased. Additionally, β-sheets that were parallel to one another and anti-parallel to one another decreased. Given the significant correlation between secondary structure and protein biological activity, the observed drop in α-helical content from 30.9% to 27.7% implies that Mb may have lost part of its biological activity following its interaction with PVC-MPs. The secondary structural alterations also demonstrated that PVC-MPs may interact with the main polypeptide chain's amino acid residues in Mb and disrupt hydrogen bonding networks, resulting in Mb adopting a less compact shape and exposing the hydrophobic core to the amino acid residues. Thus, the modification of Mb's secondary structure due to the interaction with PVC-MPs may have compromised its physiological function.

3.10. Fourier transform infrared spectroscopy (FT-IR) characterization

It is commonly recognised that FT-IR spectroscopy, which analyses hydrogen bonds and has been widely used to study the

Table 2 Secondary structure analysis of Mb with different concentrations of PVC-MPs

	3 μM Mb	3 μM Mb + 20 μg ml^{-1} PVC-MPs	3 μM Mb + 40 μg ml^{-1} PVC-MPs	3 μM Mb + 60 μg ml^{-1} PVC-MPs	3 μM Mb + 80 μg ml^{-1} PVC-MPs	3 μM Mb+ 100 μg ml^{-1} PVC-MPs
Helix (±3)	30.9%	27.0%	26.4%	29.5%	28.2%	27.7%
Anti-parallel β sheet (±2)	18.0%	13.6%	15.8%	12.4%	12.5%	15.7%
Parallel β sheet (±2)	6.2%	8.4%	9.7%	7.5%	7.9%	4.8%
β-Turn (±1)	10.8%	11.4%	11.6%	11.1%	12.2%	13.3%
Random coil (±2)	34.1%	39.6%	36.5%	39.5%	39.2%	38.5%

modification of secondary structure in proteins, is a highly effective method. Moreover, FT-IR spectra may reveal distinct peaks of many amide bands that are linked to various peptide component vibrations. The frequency of the amide bands generated by the amide I and II vibrations and the secondary structure of the protein are significantly correlated.[53,54]

Proteins' FT-IR bands can also show alterations in secondary structure connected to interactions with the protein's backbone. The amide I band (1700–1600 cm^{-1}) and the amide II band (1500–1600 cm^{-1}), which represent the stretching and bending vibrations of C=O and N–H, respectively, are the two most prominent absorption bands of Mb. We looked at the FT-IR spectra of Mb both with and without the PVC-MPs shown in Fig. 6. Following their interaction with PVC-MPs, the peak locations of the anticorrelated amide I and II modes moved, with amide I shifting from 1640.13 cm^{-1} to 1635.98 cm^{-1} and amide II shifting from 1542.18 cm^{-1} to 1507.98 cm^{-1}. In the presence of PVC-MPs, the intensities of the Amide I and II bands decreased concurrently. Given that the amide I band corresponds to the α-helix, the CD findings, which demonstrate a reduction in the proportion of α-helix after the interaction with PVC-MPs, are compatible with this. Therefore, our results provide credence to the idea that PVC-MPs can change the secondary structure of Mb.

4. Conclusions

Based on the aforementioned experimental findings, PVC-MPs were first shown to cause a noticeable conformational change in Mb. This conformational change was convectively characterised using a variety of multispectroscopic techniques, such as fluorescence spectra, UV-vis, UV-melting, CD, and FT-IR. Multispectroscopic methods have shown effective in examining the binding interactions between proteins and other compounds, primarily illuminating protein structural alterations.[21,55–59] On the other hand, we have conducted UV-vis spectroscopy by employing denaturants like urea, cu^{2+} and Mb, although we did not consider MPs as denaturants, in our results we got MPs can only alter structure of protein not a huge transition from a native state to its primary form (Fig. S11). The binding interaction of Mb with PVC-MPs was thus thoroughly and reliably observed through the use of multi-spectroscopic techniques. These results significantly reflected the binding site, binding residues, binding force, binding mode, and alteration of secondary structure, and they supported and reinforced each other's findings. Additionally, it was demonstrated that PVC-MPs had a greater affinity for binding proteins than the other two types of microplastics, PE-MPs and PS-MPs. In binding, MPs and Mb establish a strong link that holds the two molecules firmly together, frequently by chemical bonding. Conversely, adsorption is a surface phenomenon that is frequently weaker and reversible, in which molecules gather to create a film on the surface of another substance.

In conclusion, a thorough investigation has been conducted using fluorescence spectra, UV-vis, UV-melting, CD, and FT-IR to examine the binding interaction of Mb with PVC-MPs. Fluorescence experiments demonstrated that PVC-MPs may efficiently use a static quenching mode to reduce Mb's inherent fluorescence. Based on the fluorescence data, binding constants, number of binding sites, and the quenching rate constants were determined. The determined thermodynamic characteristics indicated that electrostatic interactions constituted the primary driving force for the spontaneous contact between Mb and PVC-MPs. Additionally, the results of CD and FT-IR suggested that the binding interaction of PVC-MPs with Mb resulted in changes to the microenvironment of the backbone of Mb as well as a decrease in the α-helix for the secondary structure. These changes could potentially have a negative effect on Mb's physiological functions. Therefore, based on the experimental findings, it can be deduced that PVC-MPs may bind to Mb during *in vitro* transport and metabolic activities. PVC-MPs have the capacity to bind with Mb after they have entered the blood circulation system due to its small size, disrupting the structure and physiological function of proteins in the process. Thus, this work offers important information for clarifying the possible biological toxicity of MPs at a molecular level in addition to revealing the specific binding behaviour of PVC-MPs with Mb. In the present work the three polymer types were analysed as-received and therefore differed markedly in mean hydrodynamic diameter: PVC ≈ 10.7 μm, PE ≈ 19.2 μm and PS ≈ 0.873 μm. Because the specific surface area of a sphere scales inversely with its diameter, particles that are tenfold smaller expose roughly ten-fold more surface per unit mass. So, particle size alone does not account for the binding hierarchy (PVC > PS ≈ PE) and size effects can still modulate the absolute magnitude of binding. From UV and fluorescence spectroscopy we got less change in absorption and fluorescence intensity when, PE and PS-MPs added into Mb. As, we got maximum change in absorption and fluorescence intensity when, PVC-MPs added into Mb, so we have emphasized that PVC-MPs are more toxic.

Author contributions

Souvik Ghosal and Sagar Bag: writing – original draft, visualization, validation, supervision, software, methodology, investigation, formal analysis, data curation. Sudipta Bhowmik: writing – review & editing, visualization, validation, supervision, software, resources, project administration, methodology, funding acquisition, data curation, conceptualization.

Conflicts of interest

The authors declare that they have no known competing financial interests or personal relationships that could have appeared to influence the work reported in this paper.

Data availability

The data supporting this article have been included as part of the SI.

Steady-state fluorescence of Mb in absence and presence of PE-MPs (a) and PS-MPs (b) in different concentration. [Mb] = 15 μM. [PE-MPs], and [PS-MPs] = 0-100 μg/mL, pH = 7.4, T = 298

K; UV-vis of Mb in absence and presence of PE-MPs (a) and PS-MPs (b) in different concentration. [Mb] = 3 µM. [PE-MPs], and [PS-MPs] = 0-100 µg mL^{-1}, pH =7.4, T = 298 K; Scanning Electron Microscopy of Polyethylene Microplastics, with diameter; Scanning Electron Microscopy of Polyvinyl chloride Microplastics, with diameter; Scanning Electron Microscopy of Polystyrene Microplastics, with diameter; Dynamic light scattering (DLS) analysis showing hydrodynamic size distribution of the respective MPs (a. PE, b. PVC, and c. PS, dispersed in DI-H2O at 25 °C); FT-IR Spectra of a. PE, b. PVC, and c. PS-MPs; ^{1}H-NMR spectrum of PE in DMSO-d6; ^{1}H-NMR spectrum of PVC in DMSO-d6; ^{1}H-NMR spectrum of PS in DMSO-d6; Molecular structure of a. PE, b. PVC, and c. PS-MPs; UV-vis of Mb in absence and presence of Urea and Cu2+ in different concentration. [Mb] = 3 µM. [Cu^{2+}/ Urea] = 0-30 µM , pH =7.4, T = 298 K. See DOI: **https://doi.org/10.1039/d5ra02355f**.

References

1 R. Fuller, P. J. Landrigan, K. Balakrishnan, G. Bathan, S. Bose-O'Reilly, M. Brauer, J. Caravanos, T. Chiles, A. Cohen, L. Corra and M. Cropper, *Lancet Planet. Health*, 2022, **6**, 535–547.

2 R. Xiong, F. Sauvage, J. C. Fraire, C. Huang, S. C. De Smedt and K. Braeckmans, *Acc. Chem. Res.*, 2023, **56**, 631–643.

3 EFSA Panel on Contaminants in the Food Chain (CONTAM), *EFSA J.*, 2016, **14**, 04501.

4 M. Sajjad, Q. Huang, S. Khan, M. A. Khan, Y. Liu, J. Wang, F. Lian, Q. Wang and G. Guo, *Environ. Technol. Innovation*, 2022, **27**, 102408.

5 K. Ziani, C. B. Ionită-Mîndrican, M. Mititelu, S. M. Neacșu, C. Negrei, E. Moroșan, D. Drăgănescu and O. T. Preda, *Nutrients*, 2023, **15**, 617.

6 A. Ashrafy, A. A. Liza, M. N. Islam, M. M. Billah, S. T. Arafat, M. M. Rahman and S. M. Rahman, *J. Hazard. Mater. Adv.*, 2023, **9**, 100215.

7 M. N. Issac and B. Kandasubramanian, *Environ. Sci. Pollut. Res.*, 2021, **28**, 19544–19562.

8 K. Duis and A. Coors, *Environ. Sci. Eur.*, 2016, **28**, 2.

9 P. Ju, Y. Zhang, Y. Zheng, F. Gao, F. Jiang, J. Li and C. Sun, *Sci. Total Environ.*, 2020, **734**, 139219.

10 Z. Xu, F. He, J. Yu, Z. Yang, Y. Zhu, R. Liao, R. Lyu, M. Yang, L. Zhu and M. Yang, *J. Bioresour. Bioprod.*, 2024, **9**, 185–196.

11 A. Azhagesan, N. Chandrasekaran and A. Mukherjee, *Ecotoxicol. Environ. Saf.*, 2022, **247**, 114226.

12 S. Ghosal, S. Bag and S. Bhowmik, *J. Phys. Chem. Lett.*, 2024, **15**, 6560–6567.

13 D. Barceló, Y. Picó and A. H. Alfarhan, *Environ. Toxicol. Pharmacol.*, 2023, **104**, 204.

14 Y. Yang, E. Xie, Z. Du, Z. Peng, Z. Han, L. Li, R. Zhao, Y. Qin, M. Xue, F. Li and K. Hua, *Environ. Sci. Technol.*, 2023, **57**, 10911–10918.

15 M. Brunori, *Protein Sci.*, 2010, **19**, 195–201.

16 C. Kamga, S. Krishnamurthy and S. Shiva, *Nitric Oxide*, 2012, **26**, 251–258.

17 M. W. Merx, U. Flögel, T. Stumpe, A. Gödecke, U. K. Decking and J. Schrader, *FASEB J.*, 2001, **15**, 1077–1079.

18 R. Geyer, J. R. Jambeck and K. L. Law, *Sci. Adv.*, 2017, **3**, 1700782.

19 W. J. Bowen, *J. Biol. Chem.*, 1948, **176**, 747–751.

20 J. Kundu, U. Kar, S. Gautam, S. Karmakar and P. K. Chowdhury, *FEBS Lett.*, 2015, **589**, 3807–3815.

21 P. M. Gopinath, V. Saranya, S. Vijayakumar, M. M. Meera, S. Ruprekha, R. Kunal, A. Pranay, J. Thomas, A. Mukherjee and N. Chandrasekaran, *Sci. Rep.*, 2019, **9**, 8860.

22 J. Nath, G. Banerjee, J. De, N. Dsouza, S. Sur, J. W. Scott and P. Banerjee, *J. Nanobiotechnol.*, 2025, **23**, 304.

23 N. Peez and W. Imhof, *Analyst*, 2020, **145**, 5363–5371.

24 M. D. Burman, S. Bag, S. Ghosal, S. Karmakar, G. Pramanik, R. K. Chinnadurai and S. Bhowmik, *ACS Omega*, 2023, **8**, 37054–37064.

25 J. Chen, F. Ran, Q. Chen, D. Luo, W. Ma, T. Han, C. Wang and C. Wang, *RSC Adv.*, 2019, **9**, 4463–4468.

26 C. Pelosi, C. Duce, F. R. Wurm and M. R. Tinè, *Biomacromolecules*, 2021, **22**, 1932–1943.

27 S. Singh, S. Chakma, B. Alawa, M. Kalyanasundaram and V. Diwan, *J. Hazard. Mater. Adv.*, 2023, **9**, 100225.

28 A. Klisińska-Kopacz, B. Łydżba-Kopczyńska, M. Czarnecka, T. Koźlecki, J. del Hoyo Mélendez, A. Mendys, A. Kłosowska-Klechowska, M. Obarzanowski and P. Frączek, *J. Raman Spectrosc.*, 2019, **50**, 213–221.

29 A. K. Chaudhary, K. Chaitanya and R. P. Vijayakumar, *Arch. Microbiol.*, 2021, **203**, 2183–2191.

30 A. Giannattasio, V. Iuliano, G. Oliva, D. Giaquinto, C. Capacchione, M. T. Cuomo, S. W. Hasan, K. H. Choo, G. V. Korshin, D. Barceló and V. Belgiorno, *Environ. Int.*, 2024, **190**, 108839.

31 J. Schmidt, M. Haave and W. Wang, *RSC Adv.*, 2025, **15**, 13041–13052.

32 F. H. Dos Santos Rodrigues, G. G. Delgado, T. S. da Costa and L. Tasic, *BBA Adv.*, 2023, **3**, 100091.

33 A. B. Ghisaidoobe and S. J. Chung, *Int. J. Mol. Sci.*, 2014, **15**, 22518–22538.

34 L. Tofani, A. Feis, R. E. Snoke, D. Berti, P. Baglioni and G. Smulevich, *Biophys. J.*, 2004, **87**, 1186–1195.

35 J. R. Lakowicz and G. Weber, *Biochemistry*, 1973, **12**, 4161–4170.

36 S. S. Lehrer, *Biochemistry*, 1971, **10**, 3254–3263.

37 L. Matyus, J. Szollosi and A. Jenei, *J. Photochem. Photobiol., B*, 2006, **83**, 223–236.

38 H. Mao, T. Yang and P. S. Cremer, *Anal. Chem.*, 2002, **74**, 379–385.

39 J. Rout, B. C. Swain, S. Subadini, P. P. Mishra, H. Sahoo and U. Tripathy, *Int. J. Biol. Macromol.*, 2021, **192**, 564–573.

40 D. Wu, X. Hu, Z. Cai, J. Zhang, F. Geng and H. Li, *Food Funct.*, 2023, **14**, 6422–6431.

41 A. Marty, M. Boiret and M. Deumie, *J. Chem. Educ.*, 1986, **63**, 365–366.

42 A. C. Tedesco, D. M. Oliveira, Z. G. M. Lacava, R. B. Azevedo, E. C. D. Lima, C. Gansau, N. Buske and P. C. Morais, *J. Appl. Phys.*, 2003, **93**, 6704–6706.

43 P. D. Ross and S. Subramanian, *Biochemistry*, 1981, **20**, 3096–3102.

44 A. Malik, J. Kundu, S. K. Mukherjee and P. K. Chowdhury, *J. Phys. Chem. B*, 2012, **116**, 12895–12904.

45 S. Bag, S. Ghosal, M. Mukherjee, G. Pramanik and S. Bhowmik, *Langmuir*, 2024, **40**, 10157–10170.

46 F. R. Mansoldo, E. Berrino, P. Guglielmi, S. Carradori, F. Carta, D. Secci, C. T. Supuran and A. B. Vermelho, *Spectrochim. Acta, Part A*, 2022, **267**, 120602.

47 K. R. Grigoryan and H. A. Shilajyan, *Russ. J. Bioorg. Chem.*, 2017, **43**, 255–258.

48 S. J. Millar, B. W. Moss and M. H. Stevenson, *Meat Sci.*, 1996, **42**, 277–288.

49 N. Poklar and G. Vesnaver, *J. Chem. Educ.*, 2000, **77**, 380.

50 S. M. Kelly and N. C. Price, *Curr. Protein Pept. Sci.*, 2000, **1**, 349–384.

51 L. A. Linhares and C. H. Ramos, *Appl. Biosci.*, 2023, **2**, 639–655.

52 P. Attri, M. Kim, T. Sarinont, E. H. Choi, H. Seo, A. E. Cho, K. Koga and M. Shiratani, *Sci. Rep.*, 2017, **7**, 8698.

53 A. Ioannou and C. Varotsis, *PLoS One*, 2017, **12**, e0188095.

54 K. Nienhaus, P. Palladino and G. U. Nienhaus, *Biochemistry*, 2008, **47**, 935–948.

55 A. Tamargo, N. Molinero, J. J. Reinosa, V. Alcolea-Rodriguez, R. Portela, M. A. Bañares, J. F. Fernández and M. V. Moreno-Arribas, *Sci. Rep.*, 2022, **12**, 528.

56 Y. Wang, M. Han, X. Ye, K. Wu, T. Wu and C. Li, *Microchim. Acta*, 2017, **184**, 195–202.

57 S. Hu, M. Xu, Z. Cui, Y. Xiao, C. Liu, R. Liu and X. Li, *Spectrochim. Acta, Part A*, 2023, **294**, 122511.

58 M. Xu, S. Hu, Z. Cui, C. Liu, Y. Xiao, R. Liu and W. Zong, *Chemosphere*, 2023, **323**, 138199.

59 P. Ju, Y. Zhang, J. Ding, Y. Zheng, S. Wang, F. Jiang and C. Sun, *Environ. Sci. Pollut. Res.*, 2021, **28**, 5520–5531.